Spectroscopic Characterization of Heterogeneity and Redox Effects in Zirconium−Cerium (1:1) Mixed Oxides Prepared by Microemulsion Methods

Arturo Martínez-Arias,[†] Marcos Fernández-García,[†] Ana-Belén Hungría,[†] José C. Conesa,*[,†,‡] and Guillermo Munuera*[,§]

Instituto de Catálisis y Petroleoquímica, CSIC, Campus de Cantoblanco, 28049 Madrid, Spain, and Instituto de Ciencia de Materiales de Sevilla (Centro Mixto Universidad de Sevilla-CSIC), Av. Americo Vespucio s/n, Isla de la Cartuja, 41092 Sevilla, Spain

Received: July 18, 2002; In Final Form: December 13, 2002

Two Zr−Ce (1:1 molar ratio) mixed oxide specimens, made by the same microemulsion method from different cerium precursor salts (samples ZC1 and ZC2), have been studied by a combination of physicochemical techniques. After calcination at 773 K (high surface area materials HS: $S_{BET} = 96 \pm 1$ m^2 g^{-1}) both samples present similar characteristics in XRD, Raman and TEM (pseudocubic phase t″), and XPS/Ar^+-etching experiments. This latter evidence for those materials gives a similar moderate surface enrichment in cerium and a surface anion vacancy concentration (judged from O(1s) peak shifts) lower than in CeO_2; the latter effect suggests an easy diffusion of vacancies to bulk or subsurface regions. Only EPR of adsorbed superoxide species detects a difference between both samples, evidencing in ZC2−HS the presence of small, more reducible Ce-rich bidimensional patches over a Zr-richer substrate. According to XPS/Ar^+ etching profiles, by calcination at 1173 K (LS materials; $S_{BET} < 8$ m^2 g^{-1}), surface segregation of small (ca. 3 nm) Ce-rich particles, not yet distinguishable by Raman or diffraction data and able to sustain at the surface local anion vacancy concentrations higher than in the other specimens (closer to the behavior of pure CeO_2), occurs on the ZC2 material; the ZC1 specimen, in contrast, actually becomes more homogeneous upon calcination at 1173 K. The short-scale heterogeneity indicated by EPR for sample ZC2-HS, and not for ZC1-HS, is presumed to act as a nucleus favoring formation of this new phase upon calcination. The data obtained evidence the ability of EPR and XPS/Ar^+-etching methods to reveal in these materials heterogeneity differences, not detectable by the other techniques, leading to higher reducibility of the Ce-rich surface domains in the ZC2 materials. The results are discussed in connection with the oxygen storage and buffering properties of these mixed oxides.

Introduction

Cerium−zirconium mixed oxide is a key component in the latest technology of the three-way catalysts (TWCs) used for eliminating toxic gases in automobile exhaust.[1−3] Its main role consists of providing high oxygen storage capacity (OSC) by reacting with reducing or oxidizing components present in the exhaust and thus allowing the catalysts to work efficiently even under significant gas composition oscillations around the optimum air/fuel stoichiometric value. Its main advantages over (Zr-free) cerium oxide, used for the same purpose in earlier stages of the technology,[4] lies in its higher resistance to sintering, leading to a lower decrease of the active surface during operation, and in its ability to release oxygen at moderate temperatures from deep subsurface layers and not only from the external surface (as is the case with CeO_2), thus increasing the OSC value.[3] Research in the past decade has shown that the optimum OSC behavior is observed for specimens with zirconia molar fraction $x(Zr) \cong 0.5$.[5−7]

These materials present a fluorite-type structure with seemingly random distribution of Ce and Zr in the cationic positions. For bulk materials with $0.35 < x(Zr) < 0.7$ the most stable structure (the so-called t′ phase) has a crystalline lattice distorted tetragonally (due to oxygen ion displacements within space group $P4_2/nmc$ as in tetragonal ZrO_2) with a tetragonal ratio c/a slightly above 1.00;[8] for $0.15 < x(Zr) < 0.35$ (and usually also for $x(Zr)$ up to $\cong$0.5 in the case of very small particles[5]) c/a values are indistinguishable from 1.000, although Raman spectra indicate a distortion of the atomic positions (presumably, those of the O ions, and also within the tetragonal space group $P4_2/nmc$). This is the so-called "pseudocubic" or t″ phase.[8,9]

A relevant finding in recent years is that high-temperature treatments (in particular, redox cycling) may lead in these materials to a strong increase in reducibility, an effect which may be reversed by high-temperature calcinations.[5,10] The exact explanation of this behavior is not yet known; spectroscopic data suggest subtle surface structure and composition changes.[11] Another significant observation in this respect is that high-temperature calcination (at $T \geq 1273$ K) of materials with composition close to $Ce_{0.5}Zr_{0.5}O_2$ may lead to their disproportionation into two similar solid solutions, both still of fluorite type but being strongly enriched in respectively Ce and Zr (and thus corresponding to definitely cubic and tetragonal structures);[12] thus the disordered $Ce_{0.5}Zr_{0.5}O_2$ phase is metastable against decomposition into these Ce- and Zr-enriched phases, although the basic reasons for the higher stability of these latter have not yet been elucidated in depth. This transformation, which supposedly occurs more easily when there are composition inhomogeneities (acting as nuclei for the phase disproportionation) already in the initial stages of the mixed oxide

[†] Instituto de Catálisis y Petroleoquímica, CSIC.
[‡] E-mail: jcconesa@icp.csic.es
[§] Instituto de Ciencia de Materiales de Sevilla E-mail: munuera@us.es

10.1021/jp026563+ CCC: $25.00
Published on Web 03/01/2003

preparation, may be disadvantageous for catalyst performance (since the optimum Ce:Zr ratio is no longer present) and complicate the study of the system in a relevant range of treatment temperatures. Assessment and control, already at early stages of their preparation, of the homogeneity in the composition and structure of such materials is therefore of importance. Work carried out in this laboratory and presented here indicates the abilities of some specific spectroscopies in this respect, showing also that incipient composition heterogeneities detected by them may be accompanied by significant changes in surface chemical behavior.

Experimental Section

Preparation of the Samples. Two Zr−Ce mixed oxide precursors have been prepared by the microemulsion method described in detail previously.[13] In brief, two water-in-oil emulsions where the aqueous phases are solutions of respectively $(CH_3)_4N^+OH^-$ and the relevant metal salts are mixed, and the resultant nanoparticulate precipitate is decanted, washed, and dried at 383 K. The precursors mentioned differ in that one uses cerium(III) nitrate (Aldrich, purity = 99.9%) and the other diammonium cerium(IV) nitrate (Alfa, purity = 99.9%) as source of Ce; the resulting solids are labeled respectively as ZC1 and ZC2. By calcination in air at 773 K for 2 h high surface area materials are obtained, labeled as HS. ZrO_2 and CeO_2 specimens (samples Z1-HS and C1-HS; cerium(III) nitrate was used for the latter) were prepared by the same method. Mixed oxide samples of low surface area (labeled as LS) were made from HS-type ones by further calcination at 1173 K for 6 h. The ZC1-HS specimen is the same one prepared and characterized in previous work[13−15] and the single oxides are those used in previous studies as reference materials.[15] The ZC2 samples are described here for the first time.

A specimen of zirconia-supported ceria (hereafter referred to as CeO_2/ZrO_2), used as additional reference in some experiments, was prepared by incipient wetness impregnation of ZrO_2 (kindly supplied by Degussa, VP-type experimental product, lot no. 2442−2454; $S_{BET} = 30\ m^2\ g^{-1}$) with aqueous cerium(III) nitrate so as to give a final ceria loading of 1.44 wt % (equivalent to ca. 0.25 ceria monolayers); the impregnated sample was dried and calcined at 773 K under the same conditions as for the mixed oxides. A low surface ceria sample (labeled here CeO_2-LS), used as reference in some EPR experiments, was obtained from commercial CeO_2 (Rhône-Poulenc, $S_{BET} = 109\ m^2\ g^{-1}$) by calcination in air at 1273 K for 6 h.

Characterization Techniques. Chemical analysis of Ce and Zr was performed, after dissolution by acid digestion methods,[16] by inductively coupled plasma atomic emission spectrometry (ICP-AES) in a JY model 70+ apparatus. BET surface areas were determined from N_2 adsorption isotherms in a Micromeritics 2100 automatic apparatus.

Powder XRD patterns were recorded on a Seifert diffractometer using nickel-filtered Cu Kα radiation operating at 40 kV and 40 mA and with a 0.03° step size. Fitting of the full diffractograms was carried out with the PowderCell program[17] and took into account both Cu $K\alpha_1$ and $K\alpha_2$ lines of the radiation used.

Samples for transmission electron microscopy (TEM) were prepared by crushing in an agate mortar, dispersing in isobutyl alcohol, and depositing on perforated carbon films supported on copper grids. TEM data were obtained on a JEOL 2000 FX II system (with 3.1-Å point resolution) equipped with a LINK probe for energy-dispersive spectroscopy (EDS) analysis. Electron diffraction patterns taken with the same system could be analyzed in detail by digitizing the diffraction images with a scanner and carrying out radial (angle-integrated) densitometric analysis of the circular pattern with a homemade computer program.

Infrared spectra in transmision mode were recorded at room temperature with a Nicolet 5ZDX FTIR spectrometer. Self-supporting disks of the samples (containing 10−15 mg cm^{-2}) were prepared and handled with a conventional static IR cell. Methanol adsorption (50 Torr) was performed at room temperature on samples previously outgassed at 773 K, followed by outgassing at room temperature during 15 min and finally outgassing at 373 K for 15 min.

Raman spectra (at 4-cm^{-1} resolution) were obtained with a Bruker FT-Raman instrument using the 1064-nm exciting line (400 mW beam) and taking 100 scans for every spectrum.

Photoelectron spectra were recorded with a Leybold-Heraeus spectrometer equipped with an EA-200 hemispherical electron multichannel analyzer (from Specs) and a 120-W, 30-mA Mg Kα X-ray source. Ar^+-etching treatments were carried out with a current of 6 mA and an aceleration voltage of 3.5 kV (ion current, 8 μA). This gave a sputtering yield rate of ca. 12 Å/min, according to a calibration made by using a standard Ta_2O_5 thin film electrochemically grown on a Ta foil; the ion damage (penetration) depth under these conditions was estimated as ca. 5 nm with program TRIM-90, using Monte Carlo standard calculations[18] and assuming a homogeneous $Zr_{0.5}Ce_{0.5}O_2$ composition. The powder samples (0.2 mg) were slightly pressed into small (4 x 4 mm^2) pellets and introduced into a pretreatment chamber where they were outgassed at 473 K for 2−3 h until a pressure $P < 2 \times 10^{-8}$ Torr (1 Torr = 133.33 N/m^2) was achieved; they were then moved into the analysis chamber where they were further outgassed until a pressure below 2×10^{-9} Torr was attained (2−3 h). This low pressure was maintained during all the data acquisition by ion pumping of the chamber. The outgassed samples were submitted to a standard set of treatments consisting of heating at 473 K for 1 h at 2×10^{-9} Torr followed by a two-step (2 + 13 min) Ar^+-etching at room temperature (ca. 300 K) in the preparation chamber of the instrument. After these treatments a final reoxidation was performed by heating the sample in the preparation chamber at 373 K under O_2 (1 Torr) for 30 min.

After each treatment, XP spectra in the relevant energy windows were collected for 20−90 min, depending on the peak intensities, at a pass energy of 44 eV ($1\ eV = 1.602 \times 10^{-19}$ J), which is typical of high-resolution conditions. The intensities were estimated by calculating the integral of each peak after subtraction of an S-shaped Shirley-type background with the help of UNIFIT for Windows (version 3.2) software;[19] atomic ratios were then derived by using the reported standard empirical sensitivity factors[20] for O, Ce, and Zr, the two latter being optimized for our instrument. All binding energies (BE) were referenced to the adventitious C 1s line at 284.6 eV, providing BE values within ±0.1 eV accuracy; peak u‴ characteristic of Ce^{4+} was thus obtained at 917.0 ± 0.1 eV. In the case of Ce(3d) and Zr(3d) spectra, factor analysis (FA) was used to calculate the Ce^{3+}/Ce^{4+} and Zr^{3+}/Zr^{4+} ratios in each set of spectra recorded, using the methodology developed in previous works.[21]

EPR spectra at X band ($\nu \cong 9.5$ GHz) were recorded at 77 K with a Bruker ER 200D spectrometer calibrated with DPPH ($g = 2.0036$). Portions of sample were placed in a quartz probe cell with greaseless valves, where they could be subjected to outgassing or O_2 adsorption using a conventional high vacuum

TABLE 1: Composition Data (given as zirconia molar fraction, $x(Zr) = Zr/(Ce + Zr)$) Obtained with Different Analysis Techniques for the Different ZC Samples Examined

	ZC1-HS	ZC2-HS	ZC1-LS	ZC2-LS
ICP-AES	0.48	0.46		
TEM-EDS	0.43	0.42		
XPS, 10^{-9} Torr	0.42	0.42	0.44	0.41

line (residual pressure ca. 6×10^{-3} N m^{-2}). Two types of O_2 adsorption experiment were performed, always over samples pre-outgassed at 773 K for 2 h. For the first one (denoted as adsorption at 77 K), a dose of 70 μmol of O_2 per gram of sample was admitted in the cell at 77 K followed by thorough outgassing at 77 K. For the second one (denoted as adsorption at room temperature), after admission of a dose of 70 μmol of O_2 per gram of sample at 77 K the sample is warmed to RT for 15 min and finally outgassed at room temperature during 15 min. When necessary, the spectra obtained could be computer-simulated for accurate determination of g values, and the number of paramagnetic centers detected could be quantified by double integration and comparison with a copper sulfate standard.

Results

Overall Specimen Characterization. Table 1 summarizes the results of the ICP-AES, TEM-EDS, and XPS compositional analyses of the HS samples. A good concordance is found between the Ce/Zr (=1) ratio used in preparing the precursor microemulsion and that found by chemical analysis. Data from TEM-EDS (and XPS; see more on this below) in the same table suggest a slight enrichement in ceria at the external surface of the samples.

The powder XRD patterns of the four samples are displayed in Figure 1. They show for the HS samples resolved peaks with relatively large line widths, along with a broad background of low intensity (somewhat higher in sample ZC2) in the region $2\theta < 40°$. After calcination at 1173 K, line narrowing is apparent, indicating increased crystallization of the oxides, and the broad background is still present, in particular for sample ZC2; no new lines were detected. All profiles are consistent with the *Fm*-3*m* fluorite structure and are subsequently indexed in terms of it. The corresponding lattice parameters, obtained from fittings to the full diffractgram as explained below, are summarized in Table 2; the value found for pure CeO_2, in satisfactory concordance with literature data, verifies the good calibration of the parameters obtained.

This table presents also the average crystallite size values (d), estimated from the X-ray line widths of the well-resolved and most intense (111) and (220) peaks by using Scherrer's equation. As displayed in Table 2, both ZC1-HS and ZC2-HS materials have very similar crystallite sizes, while in the corresponding LS samples the size is larger for ZC2 than for ZC1. Estimation of the surface areas which would correspond to these data, considering a single-size spherical particle model, yields for the ZC-HS samples values higher (by a factor of almost 2) than the S_{BET} areas, also reported in Table 2. This indicates some welding of the small crystallites into larger polycrystalline particles (as observed by TEM, see below) in which the grain boundaries remain inaccessible to the N_2 molecules. The effect is as expected much larger for LS samples, the mentioned factor lying in the range 15−20.

Although these XRD patterns visually agree with the sole presence of a cubic fluorite-type phase, a more detailed analysis was performed to check for more complex situations; this concentrated on the LS samples, where the smaller line widths gave more chances of discerning any such effects. Fits to the full diffractograms were thus carried out in which crystal cell parameters, Lorentzian/Gaussian ratio and angle-dependent line widths (according to the standard formula $\Delta = W + V \tan\theta + U \tan^2\theta$) of the pseudo-Voigt line shapes used and polynomial baselines were adjusted, while keeping constant Ce:Zr site occupancy ratios (equal to the chemical analysis values) and thermal parameters of the different atoms (typical values of $B = 0.2$ and 0.8 being used for cations and anions, respectively). As shown in Figure 1, for both ZC-LS samples, and especially for ZC2-LS, where higher heterogeneity would exist according to XPS data (see below), rather good fittings were achieved assuming a single phase with fluorite-type cubic symmetry. Similar or even better quality fittings (not shown) were obtained for the HS samples. Slightly better fittings (data not shown) could be obtained allowing tetragonal unit cell shapes (leading to values $c/a \approx 1.002$ for ZC1-LS and 1.008 for ZC2-LS), but this was mainly due to a marginally improved reproduction of some of the broader lines; additional shoulders or peak

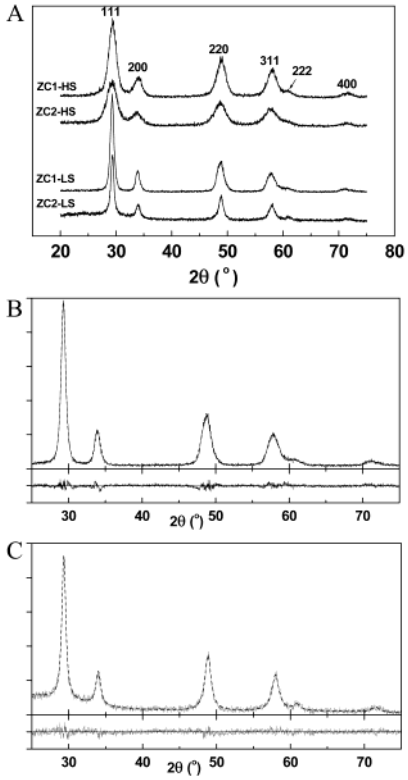

Figure 1. (A) XRD patterns of the different ceria−zirconia specimens studied. (B) Fitting of the ZC1-LS pattern to a single fluorite-type phase (see text). Dashed line, fit results; lower trace, difference residual. (C) Ibid for sample ZC2-LS.

TABLE 2: Structural and Textural Characteristics (Crystallite Size d, Cubic Cell Parameter a, and Specific Surface S_{BET}) of the Different Single-Phase Samples Examined

	XRD data		TEM data		
sample	a, Å	d,[a] nm	a,[a] Å	d, nm	S_{BET}, m^2 g^{-1}
Z1-HS		11.7			67
C1HS	5.402	8.9 ± 0.5			72
ZC1HS	5.271	5.7 ± 0.5	5.27 ± 0.03	5.2 ± 0.47[b]	96
ZC2HS	5.293	4.2 ± 0.4	5.29 ± 0.02	4.3 ± 0.37[b]	97
ZC1-LS	5.287	9.6 ± 3.2	5.27 ± 0.05	*c*	7.6
ZC2-LS	5.273	12.4 ± 2.4	5.26 ± 0.02	*c*	3.6

[a] Error figures reflect the variations in values obtained from different diffraction peaks. [b] Error figures correspond to the observed dispersion in measured particle sizes. [c] Wide particle size distributions were observed for these samples (see text).

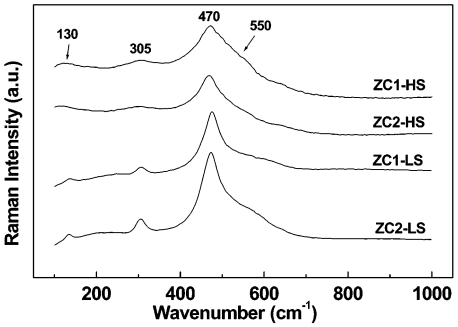

Figure 2. Raman spectra of the different ceria−zirconia specimens studied.

asymmetries did not appear in such simulations. A peak at $2\theta = 41.8°$, just faintly observable for sample ZC2-LS and allowed within space group $P4_2/nmc$ (not in the cubic fluorite symmetry), could be also reproduced in this case. In view of the high experiment−simulation agreement achieved in these fittings, no attempts were made to fit the data with a superposition of two phases having different *x*(Zr), unit cell dimensions, and peak line shapes; it was considered that any (necessarily marginal) improvement in the fit quality which might be achieved did not justify the inclusion of such large number of additional fitting parameters. In conclusion, the XRD data provide only marginal, nonconclusive indications of tetragonality in the unit cell and none of multiphasic character (although, of course, some distribution of unit cell parameters might be concealed in the diffraction line broadening). The data (Table 2) do suggest the existence of possibly significant differences in (average) unit cell parameter between the different samples; this will be referred to further below.

As shown in Figure 2, the Raman spectra were rather similar in all four samples, showing broad bands (better resolved for LS samples) at ca. 470 (with broad shoulders at ca. 550 cm^{-1}), 305, and 130 cm^{-1} superimposed on a relatively strong background; this spectrum shape is typical of the t″ phase,[9] which is thus confirmed to dominate in all specimens. No relevant difference between the samples was observed, except for the sharper peak shapes appearing in the LS-samples, which are surely due to the better crystallization.

Transmission electron micrographs of these mixed oxides are given in Figure 3. For HS samples they show a polycrystalline phase with a narrow distribution of particle sizes, clustered in agglomerates with sizes typically around 50−100 nm; for LS samples the particles appear larger and with a much broader size distribution. Electron diffraction patterns taken from selected areas of all samples show rings indexable according to a cubic fluorite structure; no special crystallite orientation relationship was observed in them. Lattice parameters (which are found to agree with the XRD results and for which no noticeable variations between different sample regions were detected) and particle sizes deduced from these data are included in Table 2. The EDS analysis (results given in Table 1) shows again a small excess of Ce, slightly higher than that obtained by ICP-AES analysis but similar to that given by XPS.

In summary, these techniques indicate that all the ZC samples seem to be constituted of single-phase solid solutions (apart from possibly some amorphous component) with compositions close to the nominal ones and a fluorite-type pseudocubic t″ structure. No specific evidence is obtained with them on compositional heterogeneity or segregation of distinct phases, even after sintering and particle growth occurring upon 6 h calcination at 1173 K, although the small changes and differences observed

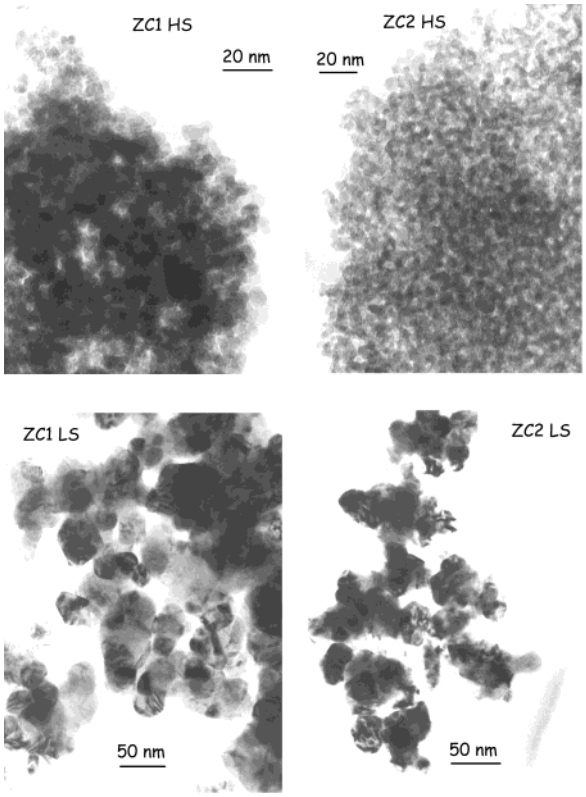

Figure 3. TEM micrographs of the different ceria−zirconia specimens studied.

in lattice parameters do suggest that there might be variations in the Ce/Zr ratio of the main observable crystalline phase.

IR spectra were obtained after adsorption of methanol on ZC samples outgassed at 773 K. For LS-type samples the data had a rather low signal-to-noise ratio, surely due to the small surface areas available, and could not be used. For HS-type samples the spectra (not shown) are similar to those obtained previously for this system;[14] the only significant difference between both samples was, besides a significantly lower overall intensity in sample ZC2-HS, a peak shift to somewhat lower frequencies in this latter, an observation that might be related to a higher Ce concentration in the topmost surface layer.[12]

XPS Spectra: HS Samples. The XPS spectrum in the Ce(3d) range obtained for sample ZC1-HS after mild outgassing (Figure 4A-a) has the shape typical of a relatively high degree of oxidation. FA shows that the fraction of Ce^{3+} amounts to ca. 32%; this is nearly 3 times higher than the ca. 12% value found under the same conditions for the C1-HS sample (spectrum not shown). Also the Zr(3d) spectrum in this case (not shown) gives a single doublet with the $E_B(3d_{5/2}) = 182.2 \pm 0.1$ eV, quite coincident with that found for the Z1-HS sample and agreeing with a Zr^{4+} state.

Sputtering with Ar^+ ions (Figure 4A-b,c) produces as expected a reduction of the material, which is only partial for a short sputtering (2 min) and rather more extensive for a 15 min bombardment; the latter spectrum is dominated by the shape typical of Ce^{3+}, the contribution of which represents 75% of the total Ce ions according to FA. Zr seems to be slighly reduced by this latter treatment; the change observed in its 4d spectrum (not shown) can be ascribed, from FA, as due to the presence of a small amount (ca. 10%) of Zr in a state with $E_B(3d_{5/2}) = 180.8 \pm 0.1$ eV (possibly Zr^{3+}), this behavior being rather similar to that observed on Z1-HS subjected to the same treatment. The Zr:Ce ratio was observed to change during sputtering; the corresponding composition data, given in Table

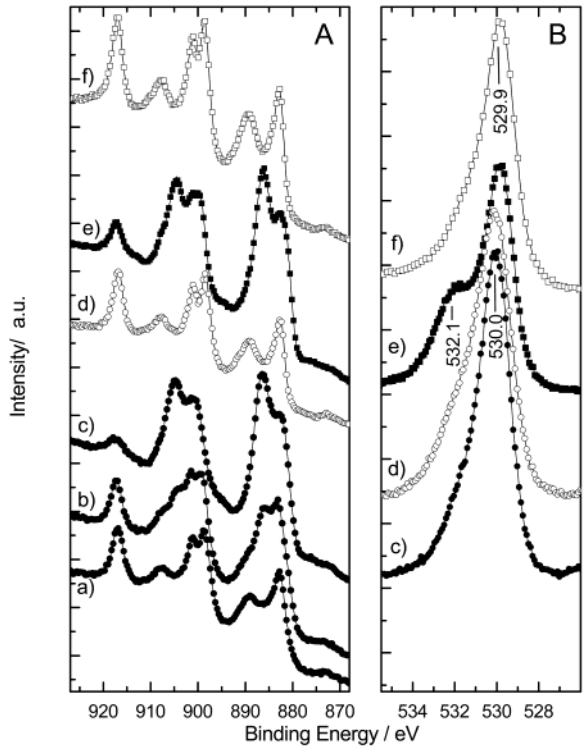

Figure 4. (A) Ce(3d) and (B) O(1s) XPS spectra: (a−d) sample CZ1-HS; (e,f) sample C1-HS. (a) After outgassing at 473 K; (b) after sputtering with Ar^+ during 2 min; (c,e) ibid., during 15 min; (d,f) after sputtering with O_2^+ during 15 min.

TABLE 3: Atomic Composition (Given as Zirconia Molar Fraction, *x*(Zr) = Zr/(Ce + Zr)) Obtained by XPS for Samples Subjected to Sputtering and Thermal/Chemical Treatments

	sample			
pretreatment	ZC1-HS	ZC2-HS	ZC1-LS	ZC2-LS
vacuum, 473 K, 10^{-9} Torr	0.42	0.42	0.44	0.41
Ar^+ etching/2 min	0.45	0.44	0.44	0.45
Ar^+ etching/15 min	0.48	0.45	0.44	0.47
O_2 (1 Torr) 373 K/30 min	0.48	0.47	0.44	0.47

3, indicate that an initial significant surface enrichment in Ce (over the chemical analysis composition value) is more or less eliminated after 15 min of sputtering.

In this extensively reduced state, the O(1s) part of the spectrum (Figure 4B-c) displays a single peak with a tail or shoulder to the higher BE side. This should not be related to the sample reduction, as a rather similar shape (Figure 4B-d) occurs if the sputtering is made with O_2^+ ions, a treatment which should keep the solid oxidized[22] as confirmed by the Ce(3d) spectrum shape (Figure 4A-d). It is not due either to carbonate species; although the corresponding C(1s) peak cannot be evaluated correctly, as it coincides with the Ce(4s) line at BE = 289.5 eV, the ratio between the integrated intensities of this latter and the Ce(3d) line is quite similar to the theoretically expected one, implying that the contribution of carbonates must be small; the same observation applies to all the other samples. Although there might be some contributions from bombardment-induced disorder to this peak broadening effect, the O(1s) shoulder in Figure 4B-c is likely to arise mainly from OH^- groups, known to appear at BE values ca. 1−1.5 eV higher than those of oxide ions[23] as is the case for the spectrum observed here. Indeed the O/(Zr + Ce) ratio derived from the XPS data is significantly higher than that corresponding to the degree of sample reduction deduced from the Ce and Zr spectra; this stoichiometry may well be due to the presence of these OH groups. It is worth mentioning here that this excess of oxygen has been found in this work to occur more than once in ZC-type materials, even after strong sputtering treatments that would be expected to lead to facile surface hydroxyl elimination. This retention of OH groups occurring some times in this system will not be further commented here; it will be subject of a separate detailed study.

A significant observation arises when comparing these results with those obtained when the same sputtering study is carried out on the reference C1-HS material (Figure 4-e,f). These spectra, which essentially agree with those obtained on thin-film CeO_2 specimens,[22] show as expected a mostly reduced/oxidized state of Ce after sputtering with Ar^+/O_2^+ ions, quite similarly to the behavior found for the ZC1-HS specimen, but the behavior in the O(1s) region differs: after Ar^+ sputtering, a distinct shoulder appears for the ceria sample at BE ca. 2.2 eV higher than the main line. This does not occur for O_2^+ sputtering and was never observed for sample ZC1-HS. Detailed study of this feature in previous work[22] has allowed us to ascribe this shoulder to O^{2-} species strongly altered by the nearby presence of a high concentration of anion vacancies. It seems thus that this latter situation does not appear for the mixed oxide sample.

If the same study is carried out on the ZC2-HS sample, the spectra (not shown) appear rather similar. The amounts of Ce^{3+} found with FA for the just outgassed and 15 min. Ar^+ ion-sputtered states are respectively 42% (somewhat higher than for ZC1-HS) and 75% (same value), while O_2^+ sputtering leaves Ce in an essentially oxidized state; the behavior of the O(1s) part of the spectrum is also rather similar to that displayed in Figure 4B-c,d.

Finally, treatment of the two Ar^+ etching-reduced samples with O_2 at 373 K (spectra not shown) produces an almost complete reoxidation of Ce^{3+} to Ce^{4+} (and of Zr^{3+} to Zr^{4+}), with an intensity increase but otherwise little shape change in the O(1s) spectrum. For sample ZC2-HS, a slight increase in the *x*(Zr) fraction (from 0.45 to 0.47) also occurs (Table 3). The difference between initial and final ratio values is thus similar for both ZC-HS samples, indicating that, at least on the average, the degree of surface enrichment in Ce is similar in both.

XPS Spectra: LS Samples. Some results obtained after the standard set of treatments on the two LS samples are included as well in Table 3. Of these samples, only in the ZC2 case does the initial outgassing at 473 K up to 10^{-9} Torr produce a visible reduction of Ce (as evidenced by the Ce(3d) spectra, not shown). Significantly, sample ZC1-LS shows in the XPS data no significant cation composition change throughout the whole set of treatments, with a constant *x*(Zr) = 0.44 value, while ZC2-LS seems to have kept a significantly Ce-enriched surface layer. To better understand this behavior, a more detailed Ar^+-etching profile analysis was carried out in this case, with a total explored depth of ca. 18 nm according to the ion gun etching yield rate. Its result is shown in Figure 5A; it confirms a quite different homogeneity in the distribution of Ce in the outer layer of the agglomerates of these two materials. It seems that, in contrast with the relatively similar behavior shown by the HS-materials, upon 1173 K treatment a homogeneization of the ZC1-LS material occurs while for ZC2-LS a distinct layer (or particles) of a Ce-rich seggregated phase appears at the surface; this can be analyzed with our previously reported methodology[24,25] as discussed in more detail below. It is worth noting here that both LS samples kept high values of the O/(Zr + Ce) ratio (above

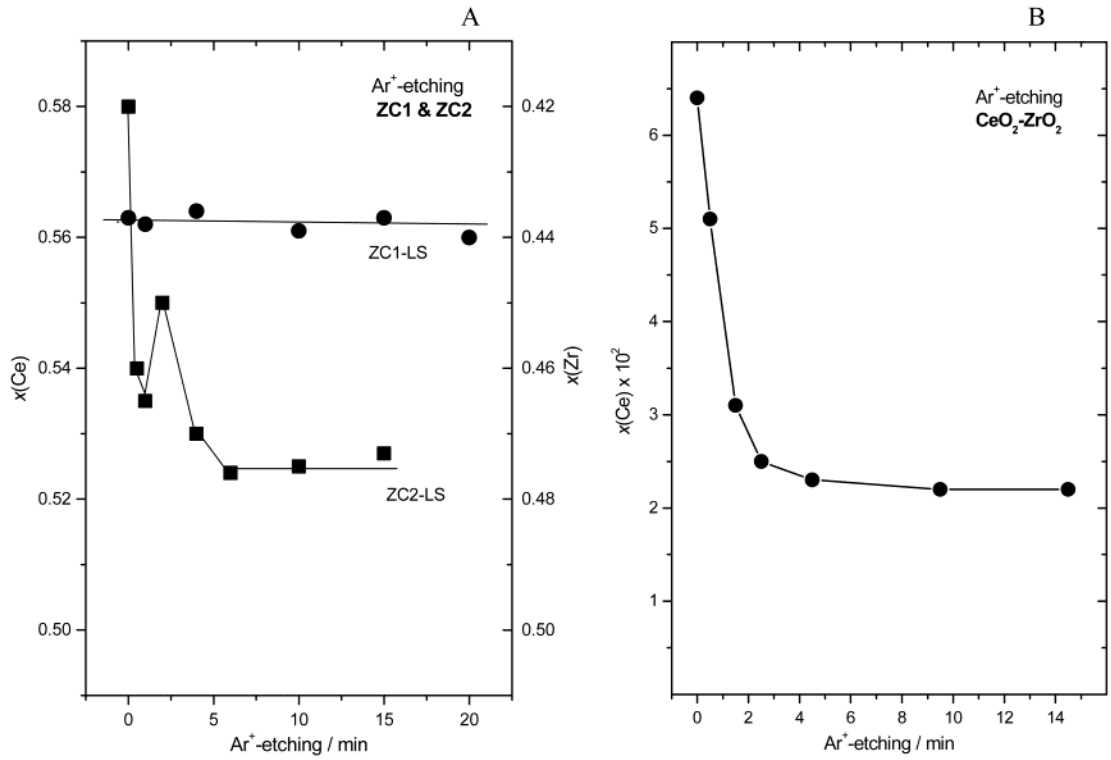

Figure 5. Profiles of the variation of cationic composition observed by XPS for increasing times of Ar^+ sputtering for samples ZC1-LS and ZC2-LS (A) and CeO_2/ZrO_2 (B).

TABLE 4: Results of XPS O(1s) Lineshape Analysis (Assuming Two Components) for Etched ZC-LS Samples

		component 1			component 2			
sample	treatment	EB[a]	fwhm[a]	% intens	EB[a]	fwhm[a]	% intens	ΔEB[a]
ZC1-LS	Ar^+ etching/2 min	530.0	1.6	41	530. 9	3.3	59	0.9
	Ar^+ etching/15 min	530.2	1.9	38	531. 0	3.5	62	0.8
ZC2-LS	Ar^+ etching/2 min	530.3	2.3	86	532. 6	1.9	14	2.3
	Ar^+ etching/15 min	530.5	2.3	87	532. 8	1.8	13	2.3

[a] In electronvolts.

2.0) even after a deep Ar^+-etching (>30 min.) producing nearly complete Ce reduction to Ce^{3+}, while for HS samples the value 1.75 could be reached, consistent with the also high degree of cerium reduction achieved. It seems thus that retention of OH^- groups is stronger in LS samples.

These results can be contrasted with those found for the CeO_2/ZrO_2 reference, displayed in Figure 5B. The sharp decay in Ce/Zr ratio indicates that ceria is here very well dispersed as a very thin layer over the ZrO_2 surface. After outgassing at T_v = 473 K, its Ce(3d) spectrum shows a ca. 50% reduction of Ce to Ce^{3+}; complete reduction of Ce to Ce^{3+} was reached after 30 s of etching, a small reduction (<10%) of Zr being observed as well after a deep Ar^+ etching.

After sputtering, the O(1s) line shapes (not shown) seemed to be intermediate between those observed for ZC and C1 HS-type samples (Figure 4B). They were analyzed by fitting them with two components (with Gaussian line shapes, for simplicity) initially located at the positions found for the strongly reduced C1-HS sample, leaving free their main parameters (intensity, BE and fwhm). The results, presented in Table 4, show that, for ZC2-LS, the starting BE parameters remained for both sputtering times almost unchanged at ca. 530.4 and 532.7 eV, with a difference of energy $\Delta E_B = 2.3$ eV similar to that found in sputtering-reduced CeO_2. By contrast, for ZC1-LS the fit converges into two peaks with a clearly lower binding energy difference ($\Delta E_B \cong 1.0$ eV), similar to that found for the O(1s) spectrum of sample ZC1-HS. Also the oxygen fraction resulting for the higher binding energy peak, included as well in Table 4, appears clearly different in both samples. Although the interpretation of the ZC1-LS situation, where the accuracy of the analysis is limited (actually one cannot certify much more than a certain asymmetry degree in the O(1s) feature), is not clear, as was also the case for the ZC-HS samples, the data do indicate a distinctly different behavior of the two LS-samples: ZC1-LS is similar in this respect to both ZC-HS samples while oxygen in ZC2-LS behaves, at least in part, more like in the CeO_2 reference. This result is consistent with the existence of CeO_2-rich regions at the surface of ZC2-LS, shown by the sputtering profile in Figure 5A, while the ZC1-LS sample remains as a quite homogeneous mixed oxide.

EPR Spectra. The main characteristics of the signals observed in the oxygen adsorption EPR experiments are summarized in Table 5; the signals found are distinguished and assigned as explained in detail in previous works.[15,26,27] Briefly, signals OC1, OC2, and OCZ are attributed to superoxide species adsorbed on cerium cations (formally describable as $Ce^{4+}-O_2^-$ species); OC1 and OC2 would be stabilized on ceria (or ceria-zirconia) particles respectively by isolated and associated vacancies, while OCZ, with features similar (including the unstability again outgassing at RT) to those of signals found for ceria highly dispersed on alumina,[27] would be due to 2-dimensional (2-D) Ce-rich patches on a less basic support. Signal OZ, with one of the g values (g_x) very close to the free-electron value ($g_e = 2.002$), is typical of $Zr^{4+}-O_2^-$ species.[15,28]

TABLE 5: Characteristics of the EPR Signals Obtained upon Oxygen Adsorption on the Samples Outgassed at 773 K

signal	EPR parameters	proposed assignment
OC1 type	$g_z = 2.031-2.030$, $g_x = 2.017$, $g_y = 2.011$ $g_{\|\|} = 2.034-2.032$, $g_\perp = 2.011-2.010$	$Ce^{4+}-O_2^-$ species formed on isolated vacancies of three-dimensional particles
OC2	$g_z = 2.042-2.039$, $g_x = 2.009-2.008$ $g_y = 2.010-2.009$	$Ce^{4+}-O_2^-$ species formed on associated vacancies of three-dimensional particles
OCZ	$g_z = 2.026-2.025$, $g_x = 2.018-2.017$ $g_y = 2.011$	$Ce^{4+}-O_2^-$ species formed on two-dimensional ceria-type patches
OZ	$g_z = 2.037, 2.032$, $g_y = 2.009$ $g_x = 2.002$	$Zr^{4+}-O_2^-$ species

Axes attribution follows criteria of previous work (refs 26, 27). For assignment details, see text.

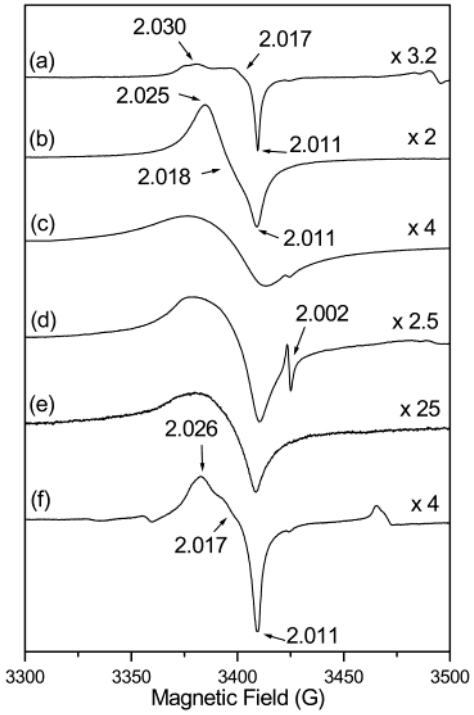

Figure 6. EPR spectra at 77 K after oxygen adsorption at 77 K (see experimental) on the samples outgassed at 773 K. (a) HS-ZC1; (b) HS-ZC2; (c) LS-ZC1; (d) LS-ZC2; (e) LS-CeO_2 reference; (f) CeO_2/ZrO_2 reference.

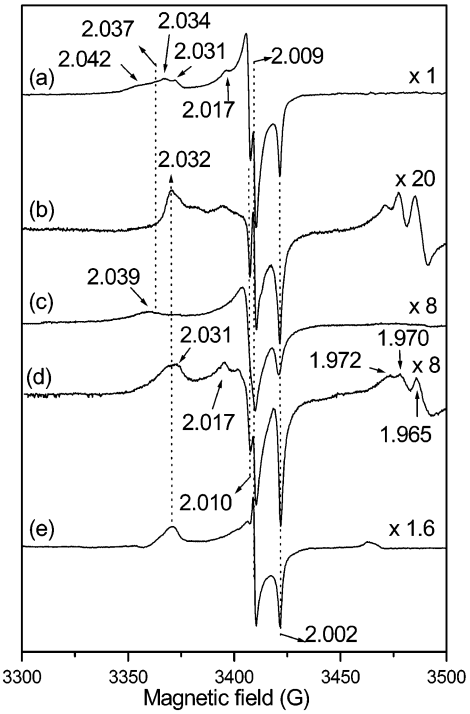

Figure 7. EPR spectra at 77 K after oxygen adsorption at room temperature (see Experimental Section for details) on the samples outgassed at 773 K. (a) HS-ZC1; (b) HS-ZC2; (c) LS-ZC1; (d) LS-ZC2; (e) CeO_2/ZrO_2 reference.

The spectra obtained after O_2 adsorption at 77 K are shown in Figure 6. Important differences are observed between both ZC-HS samples: while the spectrum of ZC1-HS is mainly constituted of overlapping of OC1-type signals, the spectrum of ZC2-HS is formed essentially by signal OCZ, which is in turn similar to the main signal shown by the CeO_2/ZrO_2 reference sample. The spectra observed for the ZC-LS samples (Figure 6c,d) are constituted by broad anisotropic signals with extrema at $g = 2.031-2.029$ and $2.010-2.008$, with minor contributions from a narrow isotropic signal at $g = 2.002$, which is present prior to O_2 adsorption and arises from defect-related centers.[15,26,27,29] It is worth noting that the amount of paramagnetic species detected in these spectra (Figure 6a-b), as quantified by double integration (which is strongly line width sensitive), is significantly higher (2−4 times more) than that found in ZC-HS samples, despite the much smaller surface area of the LS samples; this quantification also yields values higher (by ca. 50%) for sample ZC2-LS than for ZC1-LS, although the latter has a BET surface area almost twice as high as the former. Such a broad oxygen-derived signal is similar to that observed for a CeO_2-LS reference sample (Figure 6e) and corresponds most likely to OC1-type or OC2 signals broadened as a consequence of mutual spin−spin interactions between the surface paramagnetic species in these low-S_{BET} samples.

EPR spectra following O_2 adsorption (and subsequent outgassing) at room temperature are shown in Figure 7. Overall, the spectra are much sharper than in the experiments of Figure 6; this can be ascribed to a decrease in the total amount of paramagnetic species present (residual physisorbed O_2 molecules included). For sample ZC1-HS, the spectrum (Figure 7a) is constituted by the overlapping of OC1-type, OC2 and OZ signals (the latter with $g_z = 2.037$, according to the previous isolation of this signal reported in a former contribution[15]). Comparison of this spectrum with that observed for O_2 adsorption at 77 K, Figure 6a, reveals a significant increase of oxygen-derived signals upon increasing adsorption temperature, which is attributed to the existence of activated chemisorption and/or spillover processes for formation of these radicals.[15] In contrast, the spectrum observed after O_2 adsorption at room temperature for ZC2-HS (Figure 7b), which is mainly constituted by signal OZ (now with $g_z = 2.032$), shows a significantly lower overall intensity of oxygen-derived signals than that observed after O_2 adsorption at 77 K (Figure 6b). This is attributed to the low stability of the centers giving rise to signal OCZ during the outgassing step at room temperature which is included in this experiment, as the spectrum observed (at 77 K) just prior to that outgassing step (not shown) is similar in shape and intensity to that observed upon O_2 adsorption at 77 K (Figure 6b). A

similar spectrum appears for the CeO_2/ZrO_2 reference (Figure 7e), consisting mainly of signal OZ, with a much higher intensity than for ZC2-HS.

Concerning LS-type samples, the spectrum observed in this type of experiment for ZC1-LS (Figure 7c) corresponds mainly to the overlapping of signals OC2 and OZ (with $g_z = 2.037$), while ZC2-LS displays mainly the overlapping of an OC1-type signal and signal OZ (Figure 7d). It is worth noting that the intensities of the signals shown by the latter sample are higher than those displayed in the spectrum of ZC2-HS (Figure 7b), despite the lower surface area of the LS sample. Apart from this, for sample ZC2-LS the integrated intensity of the signals related to oxygen radicals is similar to that found for sample ZC1-LS, although the proportion of signal OZ in it is higher. Finally, it may be mentioned that for ZC2 samples signals appear in the $g < 2.00$ range (rightmost part of the spectra); these signals, which already appear before O_2 adsorption, can be ascribed to electrons trapped in defects, either as Zr^{3+} species or localized in anion vacancies coupled to Ce ions (the assignment of this type of signals to Ce^{3+} ions, previously proposed,[26] is more doubtful, as these species have normally very short spin relaxation times which preclude their observation at these temperatures[30]).

Discussion

Overall Structural and Textural Characteristics. The diffraction (XRD and TEM-ED) and Raman results point to the presence in all ZC samples of a single crystalline phase, in particular, phase t″ (although the XRD fittings could suggest some tetragonality of the unit cell shape, i.e., a t′-type phase, the low number of Raman peaks argues against it). The presence of phase t″ rather than the thermodynamically preferred phase t′ in these materials can be related to the very small particle dimensions.[7,31,32]

Correlations between crystal cell parameter data and Ce:Zr composition in ceria−zirconia mixed oxides, in the spirit of Vegard's law, have been presented in the literature,[33] so that one could try to compare these properties for the materials studied here. This is, however, difficult; to begin with, rather different correlations have been reported for high- and low-surface area samples.[34] Furthermore, in the first case the correlation appears rather deficient; if it were used in analyzing the present data, one would find, e.g., the rather unlikely value $x(Zr) = 0.68$ for sample ZC2-HS. In contrast, using the correlation derived for highly sintered materials,[33] one would obtain for these samples $x(Ce) = 0.53-0.59$, i.e., values in better agreement with the chemical analysis but deviating from these in ways which suggest some depletion of Zr in the crystalline phase and therefore the possible presence of some separate Zr-rich amorphous phase. It should be mentioned here that these larger-than-expected cell parameters should not be ascribed to the presence of significant amounts of Ce^{3+} ions (of larger ionic radius than Ce^{4+}), as these are not expected to be present under these preparation conditions; their presence is certainly not supported by the EPR data. Under the hypothesis (admittedly questionable) that the same correlation were valid for the HS and LS samples studied here, the change in lattice parameter observed in going from the former to the latter would imply that, upon increasing calcination temperature from 773 to 1173 K, the ZC1 material would decrease the $x(Zr)$ value while ZC2 would have the opposite behavior; i.e., upon calcination cation incorporation/segregation effects between diffracting and non-diffracting regions would occur, and these changes would be of opposite type in the two samples. If one decides, on the contrary, that these correlations cannot be used to analyze the HS samples data but that they can still be used for the LS samples, one would note, for these latter, that the smaller lattice constant observed in the ZC2 case could mean for its main crystalline component a composition somewhat depleted in Zr in comparison with the ZC1 case. In summary, results pointing to some phase heterogeneity, and variations in it depending on preparation method and calcination treatment, are suggested by the XRD technique, but beyond this no clear data corresponding specifically to a second phase are provided by it.

On the basis of the diffraction, Raman, and FT-IR data, one can therefore indirectly infer the presence of some heterogeneity (existence of some amorphous fraction with a Zr/Ce ratio different from that of the main crystallized part and also, perhaps, differences in the external enrichment in Ce between ZC1-HS and ZC2-HS samples) in these materials; but, apart from this, no indication of compositional heterogeneity within the crystallized part arises from the diffraction and Raman results, and data specific to the segregated or separate phases are not provided. Certainly, in ceria−zirconia materials with Ce/Zr ratios similar to that present here separation in Ce- and Zr-rich phases may occur upon more severe calcination treatments, leading to the presence in the diffractograms of well-resolved pairs of peaks (reflecting the correspondingly different unit cell parameters);[33] indeed some such behavior does appear in our ZC materials upon calcinations at $T = 1273$ K for extended periods of time (data not shown). Actually, it has been proposed in the literature[35] that the presence or not of such disproportionation upon a specific calcination treatment (5 h at 1273 K) may constitute a valid verification of heterogeneity in Ce,Zr mixed oxides. Although this test is clear-cut, it is, however, an indirect one, in the sense that it gives the information only through performing an irreversible material transformation, and is based essentially on assessing the kinetics of this latter; since the inherent phase change phenomena have not been characterized in enough detail yet, maybe one should not discard at present that this kinetics could be influenced by parameters other than the material heterogeneity itself and which could be different in different preparations, impairing the transferability of the method. We think it interesting to be able to assess heterogeneity features in this type of sample right in their own state, not only in a post mortem analysis. As discussed in more detail in what follows, EPR and XPS are able to provide more direct information in this respect.

Evidence of Materials Heterogeneity. According to previous studies made in one of the authors' laboratories,[24,25] for samples consisting of very small particles (oxidic or metallic) supported on a powdered support of a different composition, the results of XPS composition measurements (corresponding to the outermost surface layers) made as a function of ion sputtering duration will produce different characteristic profiles depending on several parameters (particle size, size distribution, bulk or surface incorporation, etc.). This is summarized in Scheme 1, which presents situations as may correspond to systems of a kind similar to the ZC samples studied here and in which the supported particles are distributed on the powder carrier (presumed to be formed by substantially larger particles) in three diferent ways.

Within this model, XPS/Ar^+-etching profiles of the kind displayed in Figure 5A for sample ZC1-LS correspond to systems in which all components (ZrO_2 and CeO_2 in this case) are homogeneously distributed, giving a solid solution, i.e., no specific enrichment or segregation of any of the constituents occurs at the material; this is the situation labeled a in the

SCHEME 1: Ce/(Zr + Ce) Profiles: Ar^+ Sputtering

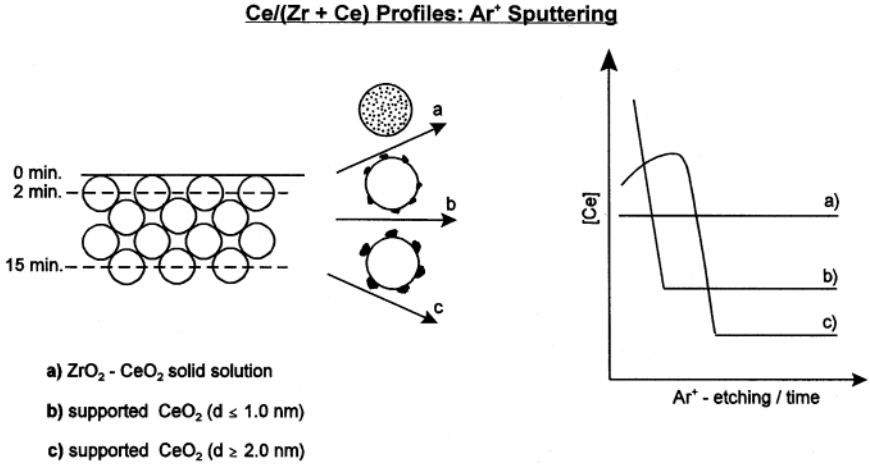

scheme. In contrast, a sharp initial decay in the composition parameter, as represented with label b in the scheme and observed in the same Figure 5A for the *x*(Ce) fraction in sample ZC2-LS, indicates that very tiny particles (or a very thin layer) of CeO_2 (or of a Ce-richer phase), here with a characteristic dimension of $d \leq 1$ nm, are present at the surface of this polycrystalline material (here formed in its main phase by clustered nanocrystallites of individual size ca. 13.3 nm according to XRD), while a maximum such as that observed in this same figure after ca. 2.5 min of etching, corresponding to the situation labeled c in the scheme, indicates the presence of other Ce-rich particles of larger size (ca. 3 nm). This implies the presence in sample ZC2-LS of a bimodal distribution of Ce-richer particles dispersed on a mixed oxide solid solution of a lower Ce concentration, i.e., a superposition of situations a, b, and c in Scheme 1 giving rise to the observed profile. It is noteworthy that the results observed upon sputtering of both HS-type ZC samples (profiles not shown, but corresponding to the data given in Table 3) are rather similar, reflecting a situation of the type labeled b in Scheme 1. This is a behavior similar to that presented by sample CeO_2/ZrO_2 (Figure 5B), although here a much smaller relative change is observed, which means that the degree of compositional difference is not so high.

Thus it seems that, from the XPS point of view, both ZC-HS samples are quite similar and characterized by a somewhat Ce-enriched external region of the nanocrystallites forming the aglomerates. It is worth noting that for these two ZC-HS samples the XPS spectra do not detect upon reoxidation significant changes in the Zr:Ce ratio, which, according to Graham et al.,[36] would indicate that the oxidation affects preferentially to a (highly reducible) segregated Ce-rich phase. These authors have shown such differences in Zr:Ce ratio (corresponding to changes in *x*(Zr) from 0.5 to 0.4 in samples sintered at $T > 1323$ K) when the domain size of the segregated CeO_2 (or Ce rich) particles (as detected by X-ray diffraction) becomes higher than the XPS sampling depth (*ca.* 1.5 ± 0.5 nm in our case). Here, only a small change (not much higher than the estimated experimental error in *x*(Zr), ca. 0.01 in our case) is observed in the ZC2-LS sample, which thus could contain a small lateral heterogeneity. So, we could conclude that, if CeO_2 seggregation has occurred in our HS samples (as suggested by data in Table 3), the size of the segregated entities must be smaller that ca. 2 nm, so that they can be hardly detected by using Graham's method. Actually this is what was observed in ref 36 for samples sintered at a lower temperature (823 K), in which case segregation was not observed by X-ray diffraction.

However, it is remarkable that, despite the apparent similarity of the two HS samples, they undergo upon calcination at 1173 K a rather different evolution: for sample ZC-1 a thorough homogeneization occurs, leading to an increase in *x*(Ce) for the dominant crystallized constituent and to a flattening of the Ar^+ sputtering profile, while for sample ZC-2 the profile shows the separation of an external layer of thicker particles richer in Ce (corresponding to a decrease in the Ce content of the main phase); i.e., a further homogeneity decrease takes place. Note that these different evolutions of both ZC samples are consistent with the different sign of the change in unit cell size, which, as revealed by XRD, occurs upon calcination; indeed, the segregation of a Ce-richer region in ZC2-LS, and not in ZC1-LS, is coherent with the smaller XRD lattice parameter in the former, which as said above implies a somewhat Zr-richer composition of the main crystalline phase. Still, the size of the domains of this segregated Ce-rich phase must be very small: they are not resolved by the XRD profile fittings, and furthermore do not give rise to clear XPS-discernible changes upon reoxidation, evidencing that the XPS/ Ar^+-etching profile method[24,25] used here is more sensitive than the procedure of Graham et al.[36] for revealing such composition heterogeneities.

An interesting correlation with these observations is found when analyzing the XPS spectra in the O(1s) region displayed by both samples after being reduced by Ar-etching. The results, summarized in Table 4, indicate that in the ZC1-LS material an important fraction (ca. 60%, although the precision of the fitting is here probably modest) of the oxide ions in the layer analyzed by XPS (ca. 2 nm thick) appear in a shifted position. This probably cannot be explained solely on the basis of surface OH species, suggesting that at least a fraction of these oxygen ions are associated to vacancies (O_v); but, if so, the modification of the anion by these must be significantly weaker than in a similarly sputtered CeO_2 specimen, since the peak shift is smaller. One possible explanation for such smaller influence of vacancies in the O(1s) spectrum could be a dilution effect of the zirconia component, the presence of which implies that the maximum density of vacancies attainable by full reduction of cerium to Ce^{3+} is lower; however, the peak shifted by ca. 2.3 eV is absent in sample ZC1-HS, even after a sputtering treatment which achieves a nearly full reduction of Ce^{4+} to Ce^{3+} (see Figure 4) and therefore implies an amount of vacancies not much different from that which is observed for the partial reduction of Ce in sample C1-HS in the same figure. The explanation may lie rather in the fast migration of vacancies into the bulk in the Ce−Zr mixed oxide (the corresponding diffusion coef-

ficient is believed to be significantly lower than in pure ceria, on the basis of TPR data[11]), which would hinder a large accumulation of such vacancies at the surface layers. By contrast, for the ZC2-LS sample the spectrum after sputtering only shows ca. 13% of perturbed anions, but these have now a higher shift (the binding energy is ca. 532.5 eV), similar to that observed for the shoulder formed in highly reduced CeO_2; this suggests the presence of regions with significantly high *x*(Ce) values, allowing at least locally high concentrations of vacancies (i.e., a pure ceria-like behavior), even if these regions might be compensated to some extent by the presence of others much richer in Zr. This agrees with the sputtering profiles indications.

While XPS reveals clear differences between the two ZC-LS samples but not between the ZC-HS specimens, an opposite situation occurs with EPR. Ce ion-stabilized O_2^- species of the kind typical of 2-D patches over a Ce-poor underlying material (giving signal OCZ) appear on sample ZC2-HS but not on sample ZC1-HS (cf. Figure 6a,b), implying that the former presents a heterogeneity at very short scale which is not present in the latter. In fact, in sample ZC2-HS only small amounts appear of the other kinds of O_2^- species, more stable against outgassing at room temperature than OCZ, as evidenced by the comparison of parts a and b of Figure 7; this implies a lower amount of the Ce ions typical of 3-D ceria (or of ceria−zirconia not depleted from Ce). It must be noted that in both ZC-HS samples Zr-stabilized O_2^- radicals (signal OZ) appear after O_2 adsorption at room temperature (in contrast with pure ZrO_2, which gives only very small amounts of such radicals in similar conditions[15]); since according to XPS, Zr^{3+} is not formed after these mild (vacuum) treatments, this implies a close proximity of Ce and Zr ions allowing some O_2^- spillover from Ce^{4+} to Zr^{4+}.

While EPR shows clear differences between samples ZC1-HS and ZC2-HS, for ZC-LS samples the dissimilarities are much less marked. The OCZ signal is no longer observed here, implying that 2-D patches have evolved into 3-D species upon high-temperature calcination. Indeed both ZC-LS materials display after O_2 adsorption at 77 K broad signals (Figure 6c,d) not much different from that displayed by similarly treated pure ceria (Figure 6e); also the spectra after adsorption at room temperature (Figure 7c,d) are similar for both ZC samples, although some diferences in g_z values, and somewhat sharper line shapes for ZC2-LS, are observed.

Thus the EPR and XP spectroscopic results are able to evidence in these materials heterogeneity in different length scales: in the ZC-HS samples, EPR shows effects at a very short scale, indicating the presence of 2-D patches in sample ZC2-HS but not in ZC1-HS, while XPS reveals for sample ZC2-LS, but not for ZC1-LS, a composition heterogeneity at a larger length scale, with segregation of small Ce-rich 3-D domains at the surface. It seems plausible that the 2-D patches in ZC2-HS act as nuclei favoring the growth of these Ce-rich 3-D domains during calcination at 1173 K (to give sample ZC2-LS). These results indicate that the ease of phase disproportionation upon high-temperature calcination in this system may depend critically on the presence of small heterogeneity differences which occur at very small scale near the surface and which are not discerned with diffraction or even by XPS experiments but can be revealed by EPR measurements. Once phase segregation begins, it can be characterized by XPS sputtering for intermediate temperature treatments which do not yield yet XRD-discernible effects, even if EPR may no longer be of much help in it.

The observed heterogeneity differences must be rooted in the preparation procedure. Although the small dimension of the droplets present in the microemulsions favors the intimate mixing of both Ce and Zr cations, for sample ZC1-HS the XPS data suggest that the Ce component may have precipitated in the microemulsion somewhat more slowly than Zr, thus leading to a higher *x*(Ce) in the last fractions of the hydrated oxide formed, which must constitute the most external layers of the solid; this would translate into a partial Ce enrichment in the outside part of the nanocrystalline mixed oxide obtained after calcination at 773 K. Examination of the Pourbaix diagrams for Zr and Ce ions in solution[37] indicates that, due to its higher acidity, Zr^{4+}, existing in solution normally as a (hydrated) ZrO^{2+} species, will precipitate upon alkali addition already at pH > 2, before the Ce ions. These diagrams also show that, while Ce^{3+} will exist in the starting solution mainly as $Ce(OH_2)_6^{3+}$ and will precipitate the insoluble $Ce(OH)_3$ around pH ≅ 7, Ce^{4+} will exist rather as a partially hydrolyzed, hydrated $Ce(OH)_2^{2+}$ species (metastable at room temperature in respect to its reduction to $Ce(OH_2)_6^{3+}$ by water) and will remain in the aqueous solution up to pH ≅ 11, precipitating as $CeO_2.xH_2O$ only under more alkaline conditions. The pH gap for precipitation of Zr and Ce ions being therefore wider for the Ce^{4+} than for the Ce^{3+} species, the formation of a more heterogeneous Zr−Ce mixed phase in the ZC2 precursor, as detected in our EPR and XPS experiments, can be explained.

Redox Characteristics. The XPS results presented here evidence one significant difference between CeO_2 and the mixed oxide in the reduction process (anion vacancy generation): at least in a reduction through sputtering such as used here, ceria may retain an important accumulation of vacancies at the topmost surface layer, while in the ceria−zirconia solid solution these do not accumulate but redistribute in subsurface layers as witnessed by the XPS O(1s) side peak. Thus it may happen that, even if the overall Ce reduction degree achieved by a given treatment in a ZC sample may be higher than in pure ceria, the latter can present locally at the surface higher levels of reduction (anion vacancy accumulation); this is likely to have influence in the oxygen activation and handling process during TWC operation.

Besides, the hetereogeneities observed at different levels have significant influence in the redox properties. Indeed, EPR shows that the dishomogeneous sample ZC2-HS behaves like ceria highly dispersed on alumina,[27] its small Ce-rich surface patches being easier to reduce at low temperature (and more stable in the reduced state) than the more homogeneous ZC1-HS. After calcination at 1173 K (LS samples) the differences are much smaller; the fact that the density of surface vacancies obtained upon outgassing at 773 K is much higher in them than in HS samples (an effect observed here to occur also with pure ceria), as deduced from the intensity and line width of the O_2^- spectra, remains unexplained and deserves a more detailed study (to be undertaken presently). A more severe reduction, such as achieved by Ar^+ etching, does reveal, however, a difference between both LS samples: in ZC2-LS part of the surface is more like pure CeO_2, allowing to establish a rather high anion vacancy concentration (reflected in the presence of an O(1s) XPS peak shifted more than 2 eV); this might have significant influence on the OSC/OBC capabilities of the material. The present study shows thus an example where these latter are influenced by the redox state of Ce in the precursor salt utilized.

Acknowledgment. Financial help from CICyT (project MAT2000-1467) is acknowledged. A.B.H. thanks the Comunidad de Madrid for a PhD grant under which her participation in this work was carried out. Thanks are due to Ms. L. N. Salamanca and Mr. F. Sánchez Constenla for performing part

of the TEM and EPR experiments, respectively, and to Mr. A. Macías for his help in recording XPS data. We thank also one of the journal referees for keen and extensive comments which have helped to improve several details of this contribution.

References and Notes

(1) (a) Ozawa, M.; Kimura, M.; Isogai, A. *J. Alloys Compd.* **1993**, *193*, 73. (b) Murota, T.; Hasegawa, T.; Azoasa, S.; Matsui, H.; Motoyama, M. *J. Alloys Compd.* **1993**, *193*, 289.

(2) Ranga Rao, G.; Kašpar, J.; Meriani, S.; di Monte, R.; Graziani, M. *Catal. Lett*. **1994**, *24*, 107.

(3) Kašpar, J.; Fornasiero, P.; Graziani, M. *Catal. Today* **1999**, *50*, 285.

(4) Heck, R. M.; Farrauto, R. J. *Catalytic Air Pollution Control*; *Commercial Technology*; Van Nostrand Reinhold: New York, 1995.

(5) Fornasiero, P.; Balducci, G.; Di Monte, R.; Kašpar, J.; Sergo, V.; Gubitosa, G.; Ferrero, A.; Graziani, M. *J. Catal*. **1996**, *164*, 173.

(6) Balducci, G.; Kašpar, J.; Fornasiero, P.; Graziani, M.; Saiful Islam, M.; Gale, J. D. *J. Phys. Chem. B* **1997**, *101*, 1750.

(7) Trovarelli, A.; Zamar, F.; Llorca, J.; de Leitemburg, C.; Dolcetti, G.; Kiss, J. T. *J. Catal*. **1997**, *169*, 490.

(8) Yashima, M.; Sasaki, S.; Yamaguchi, Y.; Kakihana, M.; Yoshimura, M.; Mori, T. *Appl. Phys. Lett.* **1998**, *72*, 182.

(9) Yashima, M.; Arashi, H.; Kakihana, M.; Yoshimura, M. *J. Am. Ceram. Soc*. **1994**, *77*, 1067.

(10) Fornasiero, P.; di Monte, R.; Ranga Rao, G.; Kašpar, J.; Meriani, S.; Trovarelli, A.; Graziani, M. *J. Catal*. **1995**, *151*, 168.

(11) Fornasiero, P.; Montini, T.; Graziani, M.; Kašpar, J.; Hungría, A. B.; Martínez-Arias, A.; Conesa, J. C. *Phys. Chem. Chem. Phys.* **2002**, *4*, 149.

(12) Colón, G.; Pijolat, M.; Valdivieso, F.; Vidal, H.; Kašpar, J.; Finocchio, E.; Daturi, M.; Binet, C.; Lavalley, J. C.; Baker, R. T.; Bernal, S. *J. Chem. Soc., Faraday Trans.* **1998**, *94*, 3717.

(13) Martínez-Arias, A.; Fernández-García, M.; Ballesteros, V.; Salamanca, L. N.; Conesa, J. C.; Otero, C.; Soria, J. *Langmuir* **1999**, *15*, 4796.

(14) Martínez-Arias, A.; Fernández-García, M.; Hungría, A. B.; Conesa, J. C.; Soria, J. *J. All. Comput.* **2001**, *323*−*324*, 605.

(15) Martínez-Arias, A.; Fernández-García, M.; Belver, C.; Conesa, J. C.; Soria, J. *Catalysis Lett.* **2000**, *65*, 197.

(16) Larrea, M. T.; Gómez-Pinilla, I.; Fariñas, J. C. *J. Anal. Atom. Spectrosc.* **1997**, *12*, 1323.

(17) Kraus, W.; Nolze, G. *Powder Cell for Windows*, v. 2.3; program described and available at Internet URL http://www.bam.de/service/download/download.htm.

(18) Ziegler, J. F.; Biscrock, J. P. *The Stopping and Range of Ions in Solids*; Pergamon Press: Elmsford, NY, 1995; p 578.

(19) Hesse, R.; Chassé, T.; Szargan, R. *Fresenius' J. Anal. Chem*. **1999**, *365*, 48.

(20) Briggs, D.; Seah, M. P. *Practical Surface Analysis by Auger and X-ray Photoemission Spectroscopies*; John Wiley & Sons: New York, 1983; p 511.

(21) Holgado, J. P.; Alvarez, R.; Munuera, G. *Appl. Surf. Sci.* **2000**, *161*, 301.

(22) Holgado, J. P.; Munuera, G.; Espinós, J. P.; González-Elipe, A. R. *Appl. Surf. Sci*. **2000**, *158*, 164.

(23) Dupin, J. C.; Gonbeau, D.; Vinater, P.; Lavasseur, A. *Phys. Chem. Chem. Phys.* **2000**, *2*, 1319.

(24) González-Elipe, A. R.; Espinós, J. P.; Fernández, A.; Munuera, G. in *Fundamental Aspects of Heterogeneous Catalysis Studied by Particle Beams* (*NATO ASI Series C 227*); Brongersma, H. H., van Santen, R. A., Eds.; Plenum Press; New York, 1991.

(25) González-Elipe, A. R.; Holgado, J. P.; Álvarez, R.; Espinós, J. P.; Fernández, A.; Munuera, G. *J. Catal.* **1991**, *130*, 627.

(26) Soria, J.; Martínez-Arias, A.; Conesa, J. C. *J. Chem. Soc., Faraday Trans*. **1995**, *91*, 1669.

(27) Martínez-Arias, A.; Fernández-García, M.; Salamanca, L. N.; Valenzuela, R. X.; Conesa, J. C.; Soria, J. *J. Phys. Chem. B* **2000**, *104*, 4038.

(28) Anpo, M.; Che, M.; Fubini, B.; Garrone, E.; Giamello, E.; Paganini, M. *Top. Catal*. **1999**, *8*, 189.

(29) Martínez-Arias, A.; Coronado, J. M.; Conesa, J. C.; Soria, J. In *Rare Earths*; Sáez Puche, R., Caro, P., Eds.; Editorial Complutense, Madrid, 1997; p 299.

(30) Wertz, J. E.; Bolton, J. R. *Electron Spin Resonance*; McGraw-Hill: New York, 1972; p 339.

(31) Gao, L.; Qiao, H. C.; Qiu, H. B.; Yan, D. S. *J. Eur. Ceram. Soc.* **1996**, *16*, 437.

(32) Schmitz, P. J.; Usman, R. K.; Peters, C. R.; Graham, C. W.; McCabe, R. W. *Appl. Surf. Sci.* **1993**, *72*, 181.

(33) Yashima, M.; Morimoto, K.; Ishizawa, N.; Yoshimura, M. *J. Am. Ceram. Soc.* **1993**, *76*, 1745.

(34) Kašpar, J.; Fornasiero, P. In *Catalysis by Ceria and Related Materials*; Trovarelli, A., Ed.; Imperial College Press: **2002;** Catalytic Science Series, Vol. 2, p 217.

(35) Fornasiero, P.; di Monte, R.; Kašpar, J.; Montini, T.; Graziani, M. *Stud. Surf. Sci. Catal.* **2000**, *130*, 1355.

(36) Graham, G. W.; Roe, C. L.; Haack, L. P.; Straccia, A. M. *J. Vac. Sci. Technol.* **2000**, *18*, 1093.

(37) Wulfsberg, G. *Inorganic Chemistry*; University Science Books: Herndon, 2000; p 294.